Nowcasting Applications of Geostationary Satellite Hourly Surface $PM_{2.5}$ Data

HAI ZHANG,[a] ZIGANG WEI,[a] BARRON H. HENDERSON,[b] SUSAN C. ANENBERG,[c] KATELYN O'DELL,[c] AND SHOBHA KONDRAGUNTA[d]

[a] *NOAA/I. M. Systems Group, College Park, Maryland*
[b] *U.S. EPA Office of Planning and Standards, Research Triangle Park, North Carolina*
[c] *Milken Institute School of Public Health, George Washington University, Washington, D.C.*
[d] *NOAA/NESDIS/Center for Satellite Applications and Research, College Park, Maryland*

(Manuscript received 23 June 2022, in final form 3 October 2022)

ABSTRACT: The mass concentration of fine particulate matter ($PM_{2.5}$; diameters less than 2.5 μm) estimated from geostationary satellite aerosol optical depth (AOD) data can supplement the network of ground monitors with high temporal (hourly) resolution. Estimates of $PM_{2.5}$ over the United States were derived from NOAA's operational geostationary satellites' Advanced Baseline Imager (ABI) AOD data using a geographically weighted regression with hourly and daily temporal resolution. Validation versus ground observations shows a mean bias of −21.4% and −15.3% for hourly and daily $PM_{2.5}$ estimates, respectively, for concentrations ranging from 0 to 1000 μg m^{-3}. Because satellites only observe AOD in the daytime, the relation between observed daytime $PM_{2.5}$ and daily mean $PM_{2.5}$ was evaluated using ground measurements; $PM_{2.5}$ estimated from ABI AODs were also examined to study this relationship. The ground measurements show that daytime mean $PM_{2.5}$ has good correlation ($r > 0.8$) with daily mean $PM_{2.5}$ in most areas of the United States, but with pronounced differences in the western United States due to temporal variations caused by wildfire smoke; the relation between the daytime and daily $PM_{2.5}$ estimated from the ABI AODs has a similar pattern. While daily or daytime estimated $PM_{2.5}$ provides exposure information in the context of the $PM_{2.5}$ standard (>35 μg m^{-3}), the hourly estimates of $PM_{2.5}$ used in nowcasting show promise for alerts and warnings of harmful air quality. The geostationary satellite based $PM_{2.5}$ estimates inform the public of harmful air quality 10 times more than standard ground observations (1.8 versus 0.17 million people per hour).

SIGNIFICANCE STATEMENT: Fine particulate matter ($PM_{2.5}$; diameters less than 2.5 μm) are generated from smoke, dust, and emissions from industrial, transportation, and other sectors. They are harmful to human health and even lead to premature mortality. Data from geostationary satellites can help estimate surface $PM_{2.5}$ exposure by filling in gaps that are not covered by ground monitors. With this information, people can plan their outdoor activities accordingly. This study shows that availability of hourly $PM_{2.5}$ observations covering the entire continental United States is more informative to the public about harmful exposure to pollution. On average, 1.8 million people per hour can be informed using satellite data compared to 0.17 million people per hour based on ground observations alone.

KEYWORDS: Atmosphere; Remote sensing; Satellite observations; Aerosols/particulates; Air quality and health

1. Introduction

The mass concentration of particulate matter with diameters less than 2.5 μm ($PM_{2.5}$) has been found to be harmful to human health. Exposure to $PM_{2.5}$ increases morbidity and mortality and can cause diseases such as acute and chronic respiratory illness, cardiovascular diseases, and even premature death (Brook et al. 2010; Miller and Xu 2018; Pope and Dockery 2006; Cohen et al. 2017; Burnett et al. 2014; Southerland et al. 2022; O'Dell et al. 2021). The United States Environmental Protection Agency (U.S. EPA) collects and distributes data from state, local, and tribal agencies through the AirNow system. AirNow includes a combination of regulatory (code 88101) and non-regulatory (code 88502) measurements at over 1000 stations, providing near-real-time hourly $PM_{2.5}$ observations. This monitoring enables EPA to disseminate to the public current air quality conditions (airnow.gov). However, measurements from surface stations have large gaps because the stations are sparse and not distributed uniformly across the United States. To fill the gaps, satellite-retrieved aerosol optical depth (AOD) along with additional data inputs are used in numerous different methods to obtain accurate surface $PM_{2.5}$ estimates (Hoff and Christopher 2009; Engel-Cox et al. 2004; Zhang et al. 2009; Gupta and Christopher 2009; Liu et al. 2005; Kloog et al. 2011; van Donkelaar et al. 2006, 2012; Hu 2009; Chu et al. 2016; Chudnovsky et al. 2012; Hu et al. 2013, 2014, 2017; Geng et al. 2018; Xiao et al. 2018; Di et al. 2019; Zhang and Kondragunta 2021; Just et al. 2020; Lee et al. 2011;

Denotes content that is immediately available upon publication as open access.

Supplemental information related to this paper is available at the Journals Online website: https://doi.org/10.1175/WAF-D-22-0114.s1.

Corresponding author: Shobha Kondragunta, Shobha.kondragunta@noaa.gov

DOI: 10.1175/WAF-D-22-0114.1

Mhawish et al. 2020; S. Park et al. 2020a,b; She et al. 2020; Song et al. 2014; Xu et al. 2015; Zheng et al. 2016). These algorithms have been developed to scale satellite AOD to daily 24-h average surface $PM_{2.5}$, making AOD-estimated $PM_{2.5}$ suitable to study long-term trends and impacts on human health. Because the statistical models are often developed using past data, the 24-h average (midnight to midnight local time) $PM_{2.5}$ data can be computed to correlate with midafternoon AOD observations from polar-orbiting satellites. When these models are applied in real time, the estimated $PM_{2.5}$ values are not representative of current conditions, however, as they represent the 24-h average. Reporting in real time requires shorter-term data to caution people in time to reduce their 24-h exposure. This is addressed by the EPA-endorsed Nowcasting method that calculates a mean $PM_{2.5}$ for the current hour by including weighted $PM_{2.5}$ values from the prior twelve hours (https://usepa.servicenowservices.com/airnow?id=kb_article_view&sysparm_article=KB0011856, accessed 13 June 2022).

Zhang and Kondragunta (2021) developed a geographically weighted regression (GWR) algorithm to estimate hourly $PM_{2.5}$ using AOD from the Advanced Baseline Imager (ABI; NOAA/NESDIS 2018; Kondragunta et al. 2020; Zhang et al. 2020). These hourly estimates of $PM_{2.5}$ can be used to fill the gaps between ground monitors and report to the public on current conditions using EPA's nowcasting method. ABI sensors are onboard Geostationary Operational Environmental Satellites (GOES) *GOES-16* and *GOES-17*, which provide high temporal resolution observations, i.e., 5 min over the continental United States (CONUS) and 10 min over the full hemispheric disk. Using ABI AOD, hourly $PM_{2.5}$ can be estimated with inputs of ground level hourly $PM_{2.5}$ monitor measurements. There are two inherent advantages of $PM_{2.5}$ estimates from GOES: 1) hourly estimates of $PM_{2.5}$ provide timely information, especially early morning estimates, which can be informative of nighttime conditions and 2) hourly estimates of $PM_{2.5}$ can be composited into daytime average values that provide expanded spatial coverage. The daytime average $PM_{2.5}$ estimate or hourly nowcasting estimate, which includes the past two hours of data to create a weighted-mean $PM_{2.5}$, are more useful in the case of smoke events when $PM_{2.5}$ variation is high and 24-h average $PM_{2.5}$ is not an effective representation of these changes.

One shortcoming of satellite AOD is that it can only be obtained during the sunlit portion of the day. Although there are some developments for nighttime AOD retrievals (Zhou et al. 2021), the data are still not available widely and algorithm work is still evolving. Despite the absence of nighttime AOD retrievals, having multiple observations from sunrise to sunset is more representative than polar-orbiting satellites, such as Visible Infrared Imaging Radiometer Suite (VIIRS; Liu et al. 2014; Zhang et al. 2016), that make only one observation in the midafternoon per day at a given location. Although there is also a morning observation from Moderate Resolution Imaging Spectroradiometer (MODIS; Levy et al., 2013), it has been on orbit for more than 20 years and will retire soon (https://www.earthdata.nasa.gov/learn/articles/modis-to-viirs-transition#:~:text=MODIS%20will%20exit%20NASA's%20'A,in%20observation%20is%20already%20underway., accessed 13 June 2022). AOD-derived $PM_{2.5}$ provides timely estimates that may be useful for air quality alerts to the public in near–real time.

In this paper, hourly, daytime, and daily $PM_{2.5}$ over the CONUS are estimated from the GWR algorithm using combined ABI AOD from *GOES-16* and *GOES-17*. Though *GOES-16* observes most of the CONUS, it views the western United States at steep angles, due to which *GOES-16* ABI AOD retrievals are less reliable (Zhang et al. 2020). *GOES-17* coverage is mostly over the Pacific Ocean and the western United States, and its retrievals are used whenever the *GOES-16* view angle exceeds 60°. For areas where both *GOES-16* and *GOES-17* observe with good view angles, an average of the two available AODs is calculated and used in the GWR algorithm. A commonly used 10-fold cross validation approach is used to evaluate the $PM_{2.5}$ estimates. The difference between daytime $PM_{2.5}$ and daily $PM_{2.5}$ is investigated using in situ AirNow data as well as the data estimated from the GWR algorithm. A rolling 3-h $PM_{2.5}$ average is also computed from hourly data to approximate the EPA's Nowcasting method and to explore the usability for exposure calculations. For exposure calculations, $PM_{2.5}$ estimates are used to deduce the number of people exposed to harmful levels of $PM_{2.5}$ ($>35\ \mu g\ m^{-3}$), which is the daily National Ambient Air Quality Standard (NAAQS) set by the EPA for 24-h average $PM_{2.5}$ (https://www.epa.gov/pm-pollution/national-ambient-air-quality-standards-naaqs-pm, accessed 8 June 2022). Even though $PM_{2.5}$ exceedances of the daily NAAQS are not based on daytime or 3-h averages, these products are being made available by NOAA to help provide real time air quality data to the public to minimize $PM_{2.5}$ exposure.

2. Data and methods

a. *ABI AOD and estimated $PM_{2.5}$ data*

AOD is a measure of the light absorbed or scattered by the total column of aerosols in the atmosphere. It is related to the $PM_{2.5}$ number concentration and optical properties and, therefore, can be used to estimate surface $PM_{2.5}$ to fill in areas without surface stations (Hoff and Christopher 2009; Martin 2008). AOD is positively correlated to $PM_{2.5}$ especially when the aerosols are in the planetary boundary layer. The relationship between AOD and $PM_{2.5}$ varies due to many factors such as planetary boundary layer height, aerosol vertical profile, aerosol optical properties, etc. (Hoff and Christopher 2009). In this work, ABI AOD is used to estimate surface $PM_{2.5}$ over the CONUS. The ABI sensor onboard the geostationary satellites *GOES-16* and *GOES-17* contains 16 bands covering the visible and infrared spectral range (Schmit et al. 2005, 2017). *GOES-16* is located at 75.2°W and *GOES-17* is located at 137.2°W. AOD at 550 nm is retrieved from ABI reflectance data in selected visible and shortwave infrared (SWIR) bands with a spatial resolution of 2 km at nadir (NOAA/NESDIS 2018; Kondragunta et al. 2020). Further bias correction is applied to the AOD data with high and medium qualities to improve AOD retrieval accuracy (Zhang et al. 2020). There is a cutoff of satellite view zenith

angle at 60°, above which AOD data are set as low quality and are not recommended. ABI AOD from *GOES-16* covers most areas of the CONUS except for several states in the western CONUS. In contrast, ABI AOD from *GOES-17* covers the western CONUS but does not cover many states in the east. By combining *GOES-16* and *GOES-17* ABI AOD, almost all the areas of the CONUS are covered, except for a small region in Montana and North Dakota (see section 3c for spatial coverage of the combined *GOES-16/17* AOD product). The ABI has different scan modes for different areas and situations. Currently, there are three scan sectors: full disk, CONUS, and mesoscale, which have temporal resolutions of 10, 5, and 1 min, respectively, for the current default "flex mode" scan mode (M6). *GOES-16* ABI AODs from the CONUS sector are used, with a temporal resolution of 5 min. For ABI AOD from *GOES-17*, full disk data with 10-min temporal resolution are used, because the full disk sector provides more coverage of the western United States compared to the CONUS sector.

Hourly composite ABI AOD data from the two satellites are combined onto the following two GOES grids: the areas to the east of 106°W are on the *GOES-16* grid and those to the west of 106°W are on the *GOES-17* grid. This combination maximizes the utility of grid spatial resolution, because the grid sizes of the *GOES-16* grid are smaller to the east of 106°W than those of the *GOES-17* grid and vice versa. In the overlapping region, AOD values from the satellite in the coarser grid are mapped to the finer grid using the nearest neighbor method. If a grid contains AOD from both sensors, they are averaged. Hourly surface $PM_{2.5}$ values are then estimated from hourly ABI AODs using the GWR algorithm, which is presented in section 2b. The period used in this study is two full years, 2020 and 2021.

The bias-corrected ABI AOD compares well with AERONET AOD, with a correlation of 0.91, a mean bias of 0.00 and a root-mean-squared error (RMSE) of 0.05 (Zhang et al. 2020). ABI AOD tends to have missing retrievals in high AOD regions, such as those with heavy smoke, for two main reasons. First, pixels with heavy smoke are sometimes misclassified as cloud by the external cloud mask algorithm and therefore no AOD retrievals are performed. Second, it is also possible that the retrieved AOD for heavy smoke pixels is higher than 5.0, which is the AOD upper bound for the AOD retrieval algorithm, so the corresponding AOD pixel is set as low quality.

1) DAILY AVERAGE AND DAYTIME AVERAGE $PM_{2.5}$

In addition to hourly $PM_{2.5}$ estimates, daily 24-h mean (hereafter daily) $PM_{2.5}$ values are estimated in two ways using the GWR algorithm: 1) the daytime mean ABI AOD and a daily 24-h mean $PM_{2.5}$ from AirNow in situ stations were used as the algorithm input to obtain daily estimated $PM_{2.5}$ (daily $ePM_{2.5}$); 2) 1300 local standard time (LST) ABI AOD (mean ABI AOD for 1300–1359 LST; representing one polar-orbiting satellite observation per day) and a daily 24-h mean $PM_{2.5}$ from AirNow in situ stations were used as the input to obtain daily estimated $PM_{2.5}$ (daily $ePM_{2.5}$_13). It should be noted that 1300 LST ABI AOD is obtained from the average of multiple observations and is therefore potentially better than a single snapshot of polar-orbiting satellite AOD. No restrictions on the number of ABI retrievals during the daytime are applied so that maximum possible spatial coverage can be achieved for daily $ePM_{2.5}$. In addition, to better represent daily AOD, daytime mean AODs cover larger areas than the 1300 LST AODs, because additional retrievals from other hours contribute to the pixels where no retrievals are available due to cloud coverage, surface brightness, etc. On average, daily composite AOD retrievals contain more than double the number of pixels of the corresponding 1300 LST AOD retrievals. Figure 1 is an example that shows the difference in coverage between the single hour mean AOD and the daytime mean AOD for a smoke case in the California and Nevada area. As can be seen in the figure, many of the gaps in the 1300 LST AOD composite are filled in the daytime AOD composite. Besides the impact of cloudiness on AOD retrieval coverage at different times of the day, another important factor is the surface reflectance dependence on the geometry over regions with little vegetation coverage. ABI does not retrieve AOD over bright surfaces. Over these areas, the surface may be bright or dark depending on the time of the day because of the differences in solar angles. In addition, the spatial inhomogeneity used for quality control of ABI AOD may be also different at different times of day due to the change in surface reflectance with respect to geometry, which also causes differences in coverage (Huff et al. 2021). Some areas have systematically lower numbers of $PM_{2.5}$ estimates than other areas and some areas have strong diurnal variations in the number of $PM_{2.5}$ estimates (see the supplement). Descriptions of different estimated $PM_{2.5}$ data and acronyms introduced here and the following sections are listed in Table 1.

Hourly estimated $PM_{2.5}$ ($ePM_{2.5}$) from ABI AOD are only available for daytime. Therefore, the average of hourly $ePM_{2.5}$ for a day represents the mean $ePM_{2.5}$ during the daytime only. It is different from the daily $ePM_{2.5}$, which is an estimate of mean 24-h $PM_{2.5}$ including both daytime and nighttime. Although ABI does not have nighttime AOD retrievals, the daily $ePM_{2.5}$ can still be estimated using daytime or 1300 LST AOD and the 24-h mean in situ $PM_{2.5}$ as described above. The daytime $ePM_{2.5}$ is obtained by averaging the hourly $ePM_{2.5}$ during a day. The daytime $ePM_{2.5}$ is used to evaluate the difference between the daytime $ePM_{2.5}$ and the daily $ePM_{2.5}$. In addition, EPA also communicates 24-h (from midnight to midnight) mean $PM_{2.5}$ using its air quality index (AQI). The AQI has six color-coded categories (https://www.epa.gov/sites/default/files/2016-04/documents/2012_aqi_factsheet.pdf, accessed 22 March 2022). Therefore, from an exposure perspective related to health impacts, daily $ePM_{2.5}$ should be used to maintain consistency with EPA standards for AQI estimates or exposure analysis.

2) 3-H COMPOSITE ACCORDING TO EPA METHOD

The EPA nowcasting method is designed such a way that it uses shorter time periods when concentrations are highly variable and relaxes to a longer average when concentrations are

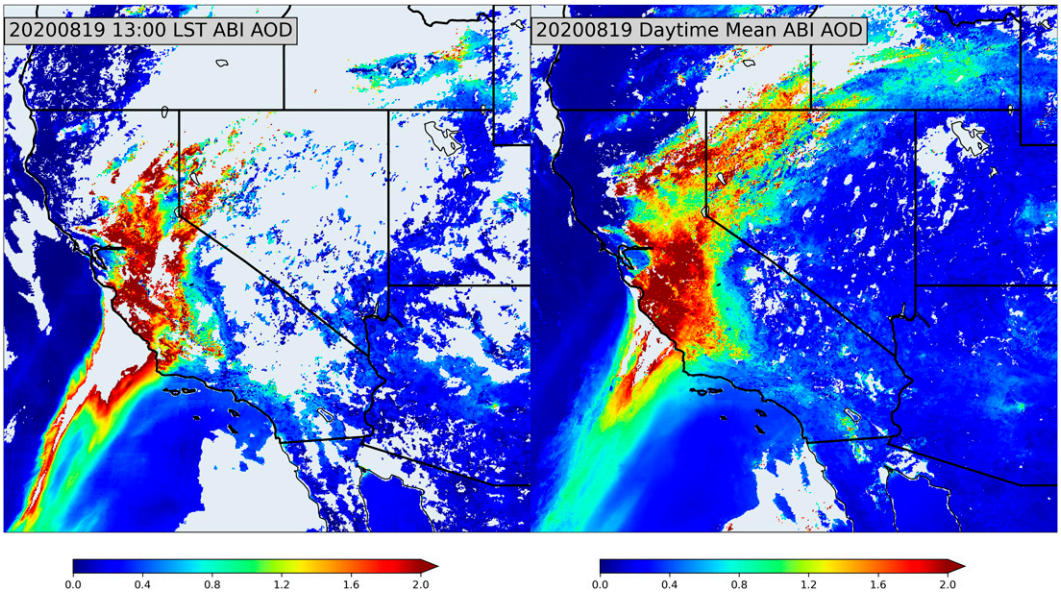

FIG. 1. ABI AOD over California and Nevada for a smoke event on 19 Aug 2020: (left) hourly AOD at 1300 LST and (right) daytime mean AOD.

stable. This approach prefers stable averages when variability is not expected to influence people's decision making outcome. To approximate the nowcast, we adopted a 3-h rolling window to calculate the current hour's $ePM_{2.5}$ that mimics EPA's approach of nowcasting during times when $PM_{2.5}$ values are changing rapidly [Eq. (1)]. When concentrations are not changing rapidly, the form of averaging will only make a small difference. Though ABI AOD data are available every five minutes for the CONUS sector, the GWR algorithm is run on hourly composites of 5-min AOD data. The hourly $ePM_{2.5}$ data are translated from coordinated universal time (UTC) to local solar time (LST) to calculate a 3-h composite (3-h $ePM_{2.5}$). For the 3-h composite $PM_{2.5}$ at a particular time step, data from that hour and the previous 2 h are included. The number of 3-h composite images in a day vary depending on location as well as season. If in a particular grid, all three observations are missing, then that value is set to a fill value:

$$PM_{2.5}\_mean(h) = mean[PM_{2.5}(i) : i \in (h, h-1, h-2) \text{ and } PM_{2.5}(i)], \quad (1)$$

where h represents the current hour.

b. AirNow data

AirNow collects data from voluntary reporting from networks of ground-based in situ surface monitors that report $PM_{2.5}$ data continuously ($oPM_{2.5}$, Table 1). The $oPM_{2.5}$ data were obtained from http://files.airnowtech.org/ (accessed 31 March 2022) for both hourly data and 24-h mean daily data. There are a total of 1244 sites over the CONUS and Canada that are used in this study for the years 2020 and 2021. Daily and hourly $oPM_{2.5}$ are reported by the Federal Reference Method (FRM), or Federal Equivalent Method (FEM) monitors, or "Acceptable $PM_{2.5}$ AQI & Speciation Mass" monitors. The regression lines between FRM and FEM are expected to

TABLE 1. Data descriptions of the $PM_{2.5}$ data.

Acronym	Explanation
$ePM_{2.5}$	Estimated $PM_{2.5}$ from ABI AOD
Daily $ePM_{2.5}$	Estimated $PM_{2.5}$ using GWR where regression parameters are between daytime ABI AOD and 24-h in situ $PM_{2.5}$
Daily $ePM_{2.5}$_13	Estimated $PM_{2.5}$ using GWR where regression parameters are between 1300 LST ABI AOD and 24-h in situ $PM_{2.5}$
Hourly $ePM_{2.5}$	Estimated $PM_{2.5}$ using GWR where regression parameters are between hourly mean AOD and hourly in situ $PM_{2.5}$
Daytime $ePM_{2.5}$	Mean of all hourly $ePM_{2.5}$ for each day
3-h $ePM_{2.5}$	3-h rolling mean of hourly $ePM_{2.5}$
$oPM_{2.5}$	In situ observed $PM_{2.5}$ from AirNow
Hourly $oPM_{2.5}$	In situ observed hourly $PM_{2.5}$ from AirNow
Daily $oPM_{2.5}$	In situ observed daily 24-h mean $PM_{2.5}$ from AirNow

have slopes within 0.9 and 1.1 and intercepts from −2 to 2 $\mu g\ m^{-3}$ (https://www.govinfo.gov/content/pkg/CFR-2008-title40-vol5/pdf/CFR-2008-title40-vol5-part53-subpartC-appC-id43.pdf, accessed 26 May 2022). In this analysis, no attempt was made to distinguish between FRM, FEM or Acceptable $PM_{2.5}$ AQI & Speciation Mass measurements. The stations are distributed unevenly and they are mostly denser in the western and eastern CONUS than in the central CONUS. Even in the east, the distribution is uneven, for example, West Virginia has only three stations, the fewest stations of any state. In addition, stations are clustered in urban and suburban regions, where population density is highest, leaving gaps in many rural areas. For the two years of data used in this study, the daily $oPM_{2.5}$ values ranged from −4 to 837 $\mu g\ m^{-3}$, and the hourly $oPM_{2.5}$ values ranged from −16 to 2629 $\mu g\ m^{-3}$. To remove outliers and potential instrument errors, we only use the hourly $oPM_{2.5}$ data within the range from −10 to 1000 $\mu g\ m^{-3}$; the number of outliers is insignificant (<100). Negative $oPM_{2.5}$ is caused by the noise of the measurement instruments when $PM_{2.5}$ is close to 0.

c. GWR algorithm to estimate $PM_{2.5}$

The GWR algorithm (Fotheringham et al. 2002; Hu et al. 2017; Ma et al. 2014; Zhang and Kondragunta 2021) is used to estimate surface $PM_{2.5}$ from ABI AOD, by building regression models locally from matchups of surface in situ $oPM_{2.5}$ data and ABI AOD data at monitor locations. Weights are assigned to differentiate the contribution of the matchup data points to the regression model such that points closer to the point of interest (i.e., the monitoring stations) have larger weights than those farther away.

In the regression model, $PM_{2.5}$ at point (i, j) is related to AOD linearly as follows:

$$PM_{2.5ij} = a_{0ij} + a_{1ij}AOD_{ij}. \quad (2)$$

The linear regression coefficients a_{0ij} and a_{1ij} are different at different locations, which are obtained through geographically weighted linear regression from the matchup of surface in situ $PM_{2.5}$ and ABI AOD data. For hourly $ePM_{2.5}$, ABI AOD data are averaged spatially for the pixels within 27.5 km of a station and then temporally for the starting hour (e.g., 0000–0059 UTC is represented by 0000 UTC; Ichoku et al. 2002). For daily $ePM_{2.5}$ estimates, ABI AODs are also averaged spatially for pixels within 27.5 km of a station and then temporally over the daytime. Therefore, the matchups for daily $ePM_{2.5}$ are between daytime ABI AOD and daily observed $PM_{2.5}$. The matchup data used are from the same time step as that when $PM_{2.5}$ is estimated.

The weight is defined as an exponential function of the distance:

$$w = \exp(-d/d_0), \quad (3)$$

where d_0 is a constant and set to be 50 km, and d is the distance between the point of interest and the matchup data point used for regression. There are other ways to select the weight, but sensitivity analysis shows that different weight selections do not cause significant difference in the resulting $ePM_{2.5}$.

Though there are many machine learning based approaches to estimate $PM_{2.5}$ using many other ancillary data, such as meteorological parameters as input, we kept our approach simple for two main reasons: 1) we run the GWR algorithm every hour in real time using AirNow $oPM_{2.5}$ and ABI AOD data, and 2) we have to generate the $ePM_{2.5}$ as soon as the data are observed so the information is disseminated to the public with low latency. If the GWR algorithm is not run in real time and is trained based on past data, then there is room for uncertainties in $ePM_{2.5}$, especially when aerosols are not well mixed and stratified in the atmosphere. Because we dynamically calculate regression parameters in near–real time, if aerosols are aloft and not located near the surface, then ground monitors capture that (i.e., surface $PM_{2.5}$ concentrations are low) and regression parameters are fit accordingly. We explored the option of using modeled boundary layer height or aerosol layer height as informed by satellites in the GWR regression but did not find a significant improvement in the accuracy of the $ePM_{2.5}$ (Fig. S3 in the online supplemental material).

d. Population density

The population dataset used in this study was derived from the American Community Survey (ACS) 2015–19 5-yr estimate by the U.S. Census Bureau. The details about the ACS can be found in https://www.census.gov/data/developers/data-sets/acs-5year.2019.html. In this study, we use the census data at census tract level. Census tracts are small, relatively permanent statistical subdivisions of a county or a statistically equivalent entity. Each census tract generally has about 4000 people, but varies from 1200 to 8000 people. The total number of census tracts in the United States was changed with decennial year. We focused our study on the 722333 census tracts in the CONUS. We assume that the population was homogeneously distributed inside a census tract. We estimate the number of exposed people by counting people in the area covered by high $ePM_{2.5}$ (>35 $\mu g\ m^{-3}$) ABI pixels. Because an ABI footprint (about 2 × 2 km^2) is larger than some areas of census tracts, we divided a satellite footprint into equal size units, i.e., about 0.1 × 0.1 km^2. These small units were gridded to 0.001° × 0.001° cells. The ratio of the total number of the high $ePM_{2.5}$ grid cells and total number of grids covered in a census tract represents the USG+ (unhealthy for sensitive groups or worse) ratio, from which we can derive the number of $ePM_{2.5}$ USG+ exposure days by multiplying the total number of people in the census tract. The USG+ corresponds to the 24-h standard for $PM_{2.5}$ from NAAQS (https://www.epa.gov/pm-pollution/national-ambient-air-quality-standards-naaqs-pm, accessed 8 June 2022).

3. Results

a. Validation of estimated $PM_{2.5}$

A 10-fold cross validation is used to validate the hourly and daily $ePM_{2.5}$ from ABI AOD (Hasti et al. 2017; Kelly et al. 2021).

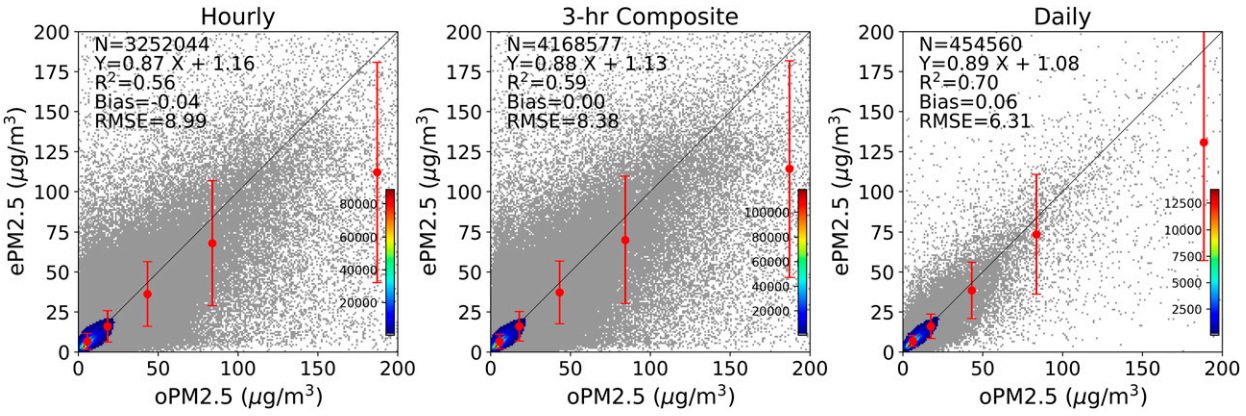

FIG. 2. Scatterplots of 10-fold cross validation of (left) hourly, (center) 3-h composite, and (right) daily $ePM_{2.5}$. The red data points are binned averages for different air quality index ranges with the vertical bars showing 1σ standard deviations.

This is a common validation approach in which $PM_{2.5}$ stations are separated into 10 random groups and the GWR algorithm is run 10 times with each group withheld once. In each round, one group of $PM_{2.5}$ is withheld and used as a validation dataset (aka, test the model) and the other nine groups are used to generate regression relations (aka, train the model). This process ensures that the data used for training are independent from those used for validation.

Figure 2 shows the scatterplots between $ePM_{2.5}$ and $oPM_{2.5}$ for hourly, 3-h composite, and daily 10-fold cross validation. The hourly $ePM_{2.5}$ have a coefficient of determination (R^2) of 0.56, bias of -0.04 $\mu g\ m^{-3}$, and root-mean-square error (RMSE) of 8.99 $\mu g\ m^{-3}$. The 3-h composite $ePM_{2.5}$ has slightly better performance than the hourly $ePM_{2.5}$, with R^2 of 0.59, bias of 0.00 $\mu g\ m^{-3}$, and RMSE of 8.38 $\mu g\ m^{-3}$. The daily $ePM_{2.5}$ have better performance than both the hourly and the 3-h composite, with R^2 of 0.70, bias of 0.06 $\mu g\ m^{-3}$, and RMSE of 6.31 $\mu g\ m^{-3}$. The differences in the performances of the three $ePM_{2.5}$ parameters are probably because the temporal averaging of AOD prior to applying the GWR algorithm reduces the noise of the data, which is caused by cloud contamination, surface brightness variation, etc. (Zhang et al. 2020). The 3-h composite has 28% more matchups than the hourly value, due to filling-in of missing data from the additional two hours. The red dots with vertical bars represent the 1-sigma standard deviation of binned data, which are separated into $PM_{2.5}$ AQI categories: good (0–12 $\mu g\ m^{-3}$), moderate (12.1–35.4 $\mu g\ m^{-3}$), USG (35.5–55.4 $\mu g\ m^{-3}$), unhealthy (55.5–150.4 $\mu g\ m^{-3}$), very unhealthy (150.5–250.4 $\mu g\ m^{-3}$), and hazardous ($\geq$250.4 $\mu g\ m^{-3}$, not shown in the figure). The statistics for these bins are shown in Table 2. All the three $ePM_{2.5}$ parameters behave similarly for the binned data: the mean biases are positive in the "good" category and those in the other categories are negative; the magnitude of the

TABLE 2. Statistics of 10-fold cross validation for different AQI categories.

	AQI ($PM_{2.5}$ range $\mu g\ m^{-3}$)	No.	Mean $oPM_{2.5}$	Mean $ePM_{2.5}$	Mean bias	Percent mean bias (%)	Std dev of bias
Hourly	Good (0–12)	2 619 018	5.62	6.53	0.91	16.2	4.94
	Moderate (12.1–35.4)	555 214	18.3	16.0	−2.3	−12.7	9.78
	USG (35.5–55.4)	44 529	43.2	36.1	−7.0	−16.3	20.2
	Unhealthy (55.5–150.4)	28 955	83.9	67.9	−16.0	−19.0	39.0
	Very unhealthy (150.5–250.4)	3125	187.1	112.1	−75.0	−40.1	68.7
	Hazardous (≥250.4)	1203	327.2	142.2	−185.0	−56.5	107.8
3-h composite	Good (0–12)	3 366 491	5.71	6.52	0.81	14.2	4.57
	Moderate (12.1–35.4)	710 356	17.9	16.0	−2.0	−10.9	9.18
	USG (35.5–55.4)	51 560	43.2	37.2	−6.0	−13.8	19.6
	Unhealthy (55.5–150.4)	34 917	84.3	70.0	−14.3	−17.0	39.6
	Very unhealthy (150.5–250.4)	3763	187.1	114.2	−72.9	−39.0	67.6
	Hazardous (≥250.4)	1490	328.6	155.6	−173.1	−52.6	113.3
Daily	Good (0–12)	371 465	6.22	6.84	0.62	9.9	3.29
	Moderate (12.1–35.4)	75 588	17.5	16.0	−1.5	−8.8	7.66
	USG (35.5–55.4)	4172	43.1	38.5	−4.6	−10.7	17.6
	Unhealthy (55.5–150.4)	2881	83.5	73.4	−10.1	−12.1	37.2
	Very unhealthy (150.5–250.4)	325	188.4	130.7	−57.7	−30.6	73.6
	Hazardous (≥250.4)	129	330.6	199.4	−131.2	−39.6	114.8

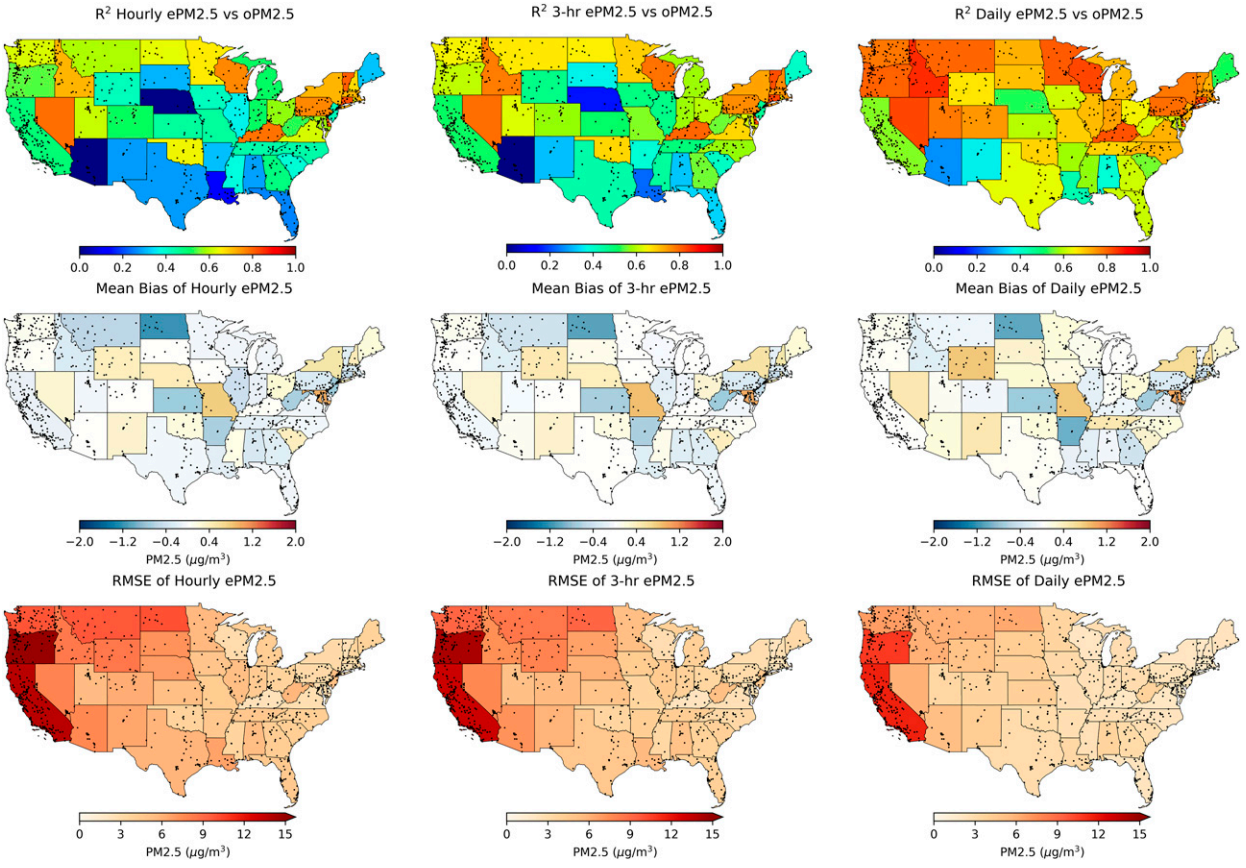

FIG. 3. The R^2, mean bias, and RMSE of 10-fold cross validation over CONUS by state. The dots represent the locations of ground $PM_{2.5}$ stations.

negative mean bias increases with increasing $PM_{2.5}$ concentrations. On the other hand, the daily $ePM_{2.5}$ values have reduced magnitudes of mean bias compared to the hourly and 3-h composite estimates at high $PM_{2.5}$ ranges.

As reported by Zhang and Kondragunta (2021), there are several reasons for the large negative bias at high $PM_{2.5}$ concentrations. One of the main reasons is that the high AOD retrievals are usually missing, especially in heavy smoke regions, which are caused by the misclassification of the cloud mask, over-screening for residual cloud contamination using the spatial variability test, or the AOD retrieval out-of-range flag (AOD > 5.0; NOAA/NESDIS 2018). The large spatial variability of AOD at high $PM_{2.5}$ concentrations also introduces uncertainty in the matchups, which use mean AOD in an area with a radius of 27.5 km from a site. In addition, high $PM_{2.5}$ values are not very prevalent because $PM_{2.5}$ air quality in the United States is generally clean, with higher concentrations observed only during smoke transport from fires or dust storms. As a result, the regression model is trained mostly by low $oPM_{2.5}$-AOD matchups. While artificial oversampling techniques such as the synthetic minority oversampling technique (SMOTE) may help minimize the low bias for high $PM_{2.5}$ values, the estimates are still biased low (Vu et al. 2022).

We further validated the $ePM_{2.5}$ values in a spatial context. How does the GWR algorithm perform when not only surface type changes drastically, but also when aerosol concentrations are drastically different? As we move from the eastern United States to the western United States, the surface reflectance increases due to dry land, which impacts ABI AOD retrievals. Also, high concentrations of $PM_{2.5}$ from wildfire smoke are observed more often in the western United States. Though fires also occur in the southeastern United States, they do not cause the extremely high, widespread $PM_{2.5}$ concentrations as observed in the western United States (Li et al. 2021; O'Dell et al. 2021). We show in section 3c that the annual mean AOD and the number of days with $PM_{2.5}$ concentrations greater than 35 $\mu g\ m^{-3}$ in the southeastern United States are similar to those in the areas with very few fire/smoke events and are much smaller than those in the western U.S. fire/-smoke region (Figs. 7 and 8).

Figure 3 shows the maps of validation statistics by state over the CONUS, including R^2, mean bias, and RMSE, for the hourly $ePM_{2.5}$, 3-h composite $ePM_{2.5}$, and the daily $ePM_{2.5}$. As expected, the performances from worst to the best are in the order of hourly, 3-h composite, and daily $ePM_{2.5}$. The performance of hourly and 3-h composite $ePM_{2.5}$ are close, with 3-h composite a little better. The R^2 of both the

hourly and 3-h $ePM_{2.5}$ ranges from close to 0 to 0.83, while R^2 of the daily $ePM_{2.5}$ ranges from 0.26 to 0.86. The 3-h $ePM_{2.5}$ has higher R^2 in some states than the hourly $ePM_{2.5}$. In general, the northern states have higher R^2 than the southern states. The three $ePM_{2.5}$ parameters have similar mean bias values, with a range from -1 to 1 $\mu g\ m^{-3}$.

The hourly and 3-h composite $ePM_{2.5}$ have higher RMSE than the daily $ePM_{2.5}$. RMSEs for the hourly $ePM_{2.5}$ are in the range of 2.1–14.8 $\mu g\ m^{-3}$, RMSEs for the 3-h composite $ePM_{2.5}$ are in the range of 2.1–14.1 $\mu g\ m^{-1}$, and RMSEs for the daily $ePM_{2.5}$ are in the range of 1.8–11.6 $\mu g\ m^{-3}$. The western states have higher RMSE than the eastern states, with the states of California and Oregon having the highest RMSEs. This is likely because frequent smoke from wildfires in these regions causes higher $PM_{2.5}$ than in the eastern United States. The GWR algorithm tends to have larger negative bias and larger RMSE for higher $PM_{2.5}$.

The distribution of the $PM_{2.5}$ ground stations is not uniform, as shown by the black dots to identify monitor locations in each state (Fig. 3). Some states only have a few stations and the statistics derived from them may not be representative if $PM_{2.5}$ concentrations are driven by mesoscale events as opposed to synoptic scale events. For example, the stations in Nevada are all located near the boundaries at the southwestern the southern corners of the state, where the largest urban centers are, and there are no stations in the middle of the state. However, from Fig. 3 there is no obvious relation between the performance and the station density.

Because the regression model is built using the $oPM_{2.5}$ and AOD matchup data close to the point of interest, the accuracy of $ePM_{2.5}$ can also be related to the spatial density of the AirNow sites or the distance of the closest site to the point of interest. Figure 4 shows the errors of the hourly $ePM_{2.5}$ versus the distance of the nearest site using the 10-fold cross validation for different AQI categories. The data are separated into bins with the same number of points, and the mean and standard deviation are calculated for each bin. There are no obvious variations of $ePM_{2.5}$ errors with respect to the distance of the nearest site for the categories of good, moderate, USG, and unhealthy. For the very unhealthy and hazardous categories, there are increases in the negative bias from 0 to 50 km, i.e., from -25 to -100 $\mu g\ m^{-3}$ for very unhealthy and from -50 to -200 $\mu g\ m^{-3}$ for hazardous categories. The standard deviations of errors do not vary much for these two categories, which are about 50 $\mu g\ m^{-3}$ and 100 $\mu g\ m^{-3}$ respectively. This is likely because of the mesoscale variability of $PM_{2.5}$, especially in episodic situations of smoke from fires and dust storms. We found that the scale length of AOD on low pollution days is about 100 km, and when pollution levels are varying dramatically over short distances, as can occur during smoke transport (vertical lofting and horizontal transport at higher altitudes not impacting the surface), including monitor data from distances of 50–100 km can lead to poor regression relations.

The relation of the hourly $ePM_{2.5}$ errors to the surface type is also investigated. For each site, the AOD pixels within a circle with a radius of 27.5 km are analyzed, and the surface type with maximum pixel numbers is assigned to be the surface type of the site, using the National Land Cover Database (NLCD) for the CONUS from https://www.mrlc.gov (accessed 28 March 2022). Figure 5 shows the histogram of land cover surface types for the AirNow sites and the hourly $ePM_{2.5}$ errors versus surface types. From the figure, the median hourly $ePM_{2.5}$ errors for each type do not have noticeable variation. The variations of hourly $ePM_{2.5}$ errors range from 5 to 14 $\mu g\ m^{-3}$. Barren land has the largest variation of about 14 $\mu g\ m^{-3}$, but there is only one site belonging to this type. The rest of the surface types have hourly $ePM_{2.5}$ error variations ranging from 5 to 10 $\mu g\ m^{-3}$. Of these, shrub/scrub, grassland/herbaceous, evergreen herbaceous wetland, and medium/high intensity developed have higher variations ($\sim$10 $\mu g\ m^{-3}$). Deciduous forest and open space developed have lower variations ($\sim$5 $\mu g\ m^{-3}$).

b. *Analysis of AirNow $PM_{2.5}$ data*

Because satellite sensors can only retrieve daytime AOD, AODs used to calculate daily $ePM_{2.5}$ do not represent a 24-h mean as do the 24-h means of $oPM_{2.5}$ data. If AOD retrievals from polar-orbiting satellites are used, such as VIIRS on board *SNPP* and *NOAA-20*, daily AODs are represented by observations at about 1330 LST. If AOD retrievals from geostationary satellites are used, such as ABI on *GOES-16* and *GOES-17*, daily AODs are represented by the mean of all daytime hourly observations. The $oPM_{2.5}$ values from AirNow are reported as 1-h means from which 24-h means are calculated. Therefore, these AirNow data are used here to analyze the representativeness of observations made only during the sunlit portion of the day.

The correlation and differences between hourly $oPM_{2.5}$ at 1300 LST and daily $oPM_{2.5}$, as well as those between daytime $oPM_{2.5}$ and daily $oPM_{2.5}$, are analyzed. The hourly $oPM_{2.5}$ at 1300 LST is the average $oPM_{2.5}$ for the hour 1300–1359 LST, which covers the 1330 LST polar-orbiting satellite sensor (e.g., VIIRS) overpass time. The daytime hours are different for different seasons, which roughly approximates the time periods that ABI AOD has retrievals with appropriate solar angles. The daytime is defined as local standard time of 0900–1500 for winter (December–February), 0800–1600 for spring and fall (March–May and September–November), and 0600–1800 for summer (June–August), and daily is defined as the 24-h average of observations in local time.

Figure 6 shows the CONUS maps of correlation, mean difference, and root mean squared difference (RMSD) between $oPM_{2.5}$ at 1300 LST and daily $oPM_{2.5}$, and between the daytime $oPM_{2.5}$ and the daily $oPM_{2.5}$. The data show that 1300 LST $oPM_{2.5}$ has a larger difference with the daily $oPM_{2.5}$ than the daytime $oPM_{2.5}$ has with the daily $oPM_{2.5}$. The correlations between the 1300 LST $oPM_{2.5}$ and the daily $oPM_{2.5}$ range from 0.46 to 0.95, while those between the daytime $oPM_{2.5}$ and the daily $oPM_{2.5}$ range from 0.68 to 0.98. The correlations for the daytime $oPM_{2.5}$ are higher than those for the 1300 LST $oPM_{2.5}$ in all states. Both the 1300 LST $oPM_{2.5}$ and the daytime $oPM_{2.5}$ are lower than the 24-h mean $PM_{2.5}$ in most states, with a magnitude of around -1 and -0.5 $\mu g\ m^{-3}$, respectively; inclusion of higher $oPM_{2.5}$ values during the

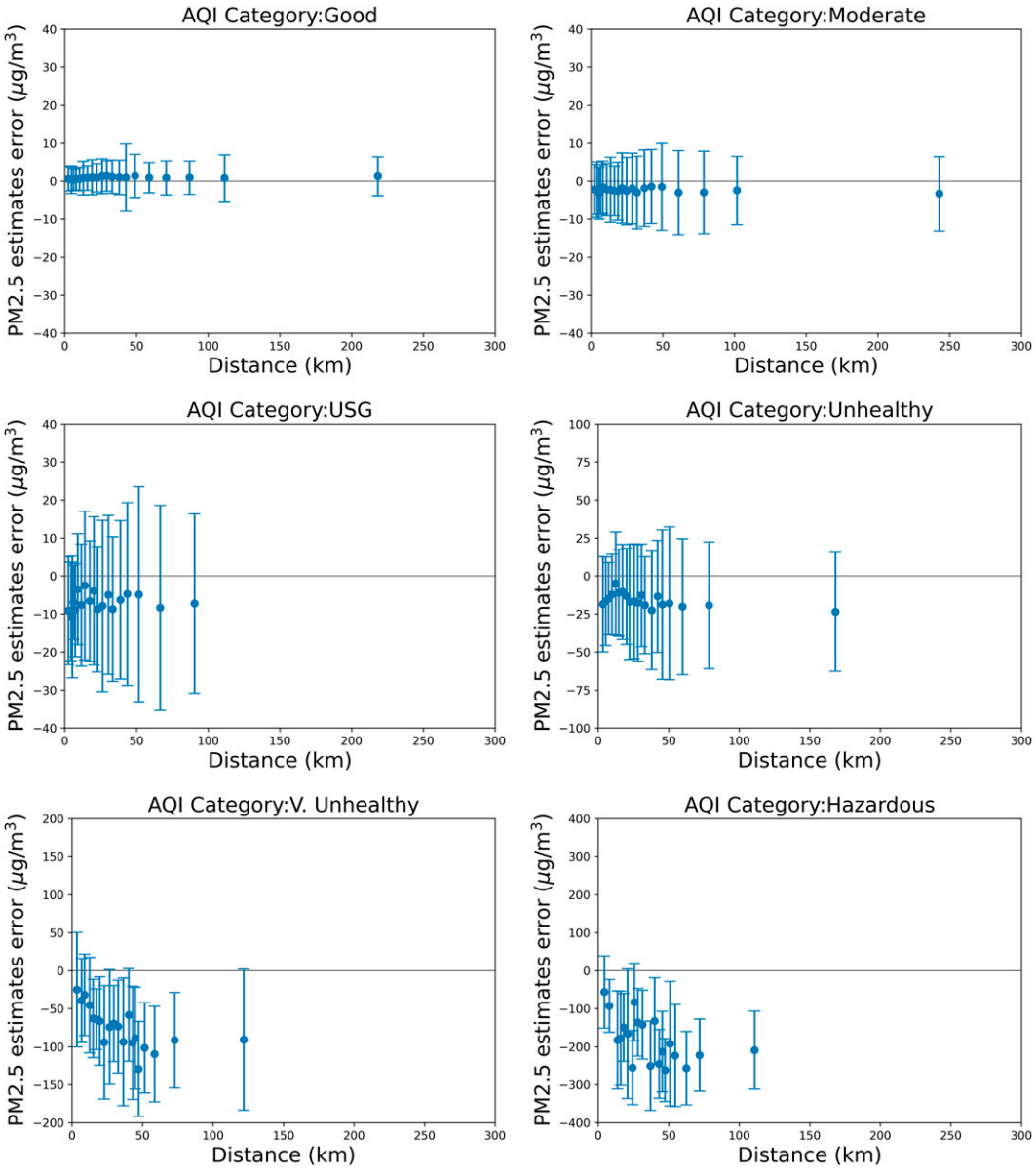

FIG. 4. Hourly $ePM_{2.5}$ errors vs distance of nearest site. The dots represent the averages of hourly $ePM_{2.5}$ minus $oPM_{2.5}$, and the bar ranges represent ±1 standard deviation of the differences.

nighttime due to a shallow boundary layer is likely the reason. RMSDs between the 1300 LST $PM_{2.5}$ and the daily $oPM_{2.5}$ (2.5–11.8 $\mu g\ m^{-3}$) are also higher than those between the daytime $oPM_{2.5}$ and the daily $oPM_{2.5}$ (1.7–6.5 $\mu g\ m^{-3}$). The distributions of the correlation coefficients and RMSDs are similar to those of R^2 and RMSE in Fig. 3, i.e., the correlations are higher in the northern states than those in the southern states, and RMSDs are higher in the western states than those in the eastern states, with the highest values in California and Oregon. The temporal inconsistency between the AOD selection (i.e., daytime AOD versus 1300 LST AOD) to correlate with the daily $oPM_{2.5}$ in the GWR algorithm is a source of uncertainty in estimating the daily $PM_{2.5}$.

The comparisons of the 1300 LST $oPM_{2.5}$ and the daytime $oPM_{2.5}$ to the daily $oPM_{2.5}$ show that it is more accurate to estimate daily $PM_{2.5}$ using the daytime $PM_{2.5}$ than using measurements from a single time step. This result indicates that using AOD from geostationary satellites with higher temporal resolution can potentially estimate daily $PM_{2.5}$ more accurately than using AOD from polar-orbiting satellites, which have only one or two overpasses per day.

c. *Analysis of ABI $ePM_{2.5}$ data*

The daily $ePM_{2.5}$ from ABI AOD are averaged and annual means for the years 2020 and 2021 are obtained, as shown in Fig. 7. Similar patterns of the annual mean $PM_{2.5}$ are observed

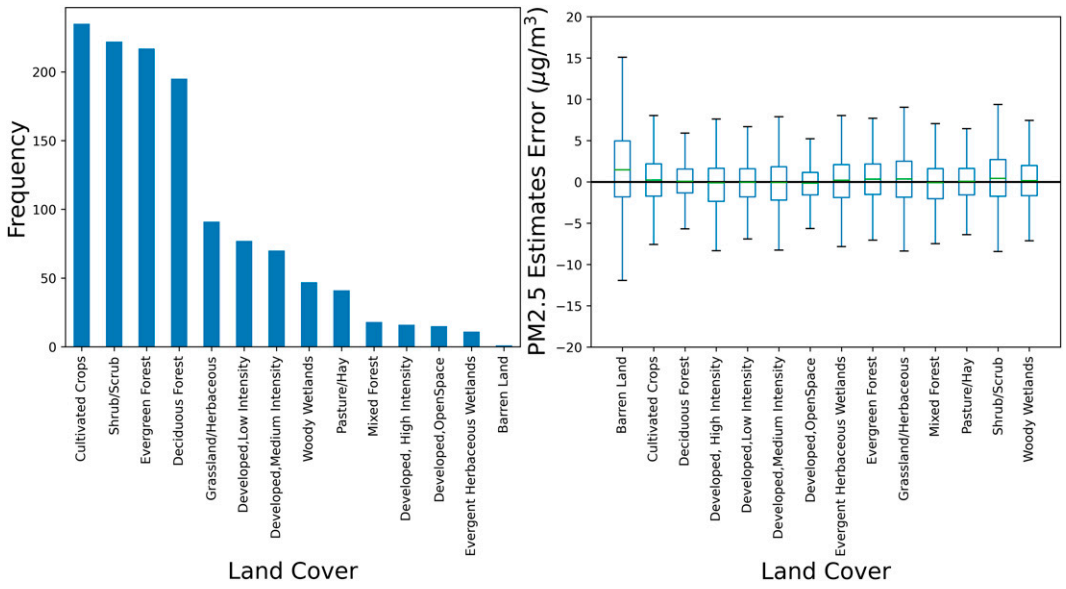

FIG. 5. Histogram of land cover for (left) AirNow sites and (right) hourly $ePM_{2.5}$ errors vs surface type.

in both years: states in the western United States including California, Nevada, Oregon, and Washington, have high annual mean $ePM_{2.5}$, i.e., higher than 12 $\mu g\ m^{-3}$ in many regions and as high as 20–30 $\mu g\ m^{-3}$ in some regions; most of $ePM_{2.5}$ values in the central and eastern states are much lower, i.e., below 12 $\mu g\ m^{-3}$. The higher $ePM_{2.5}$ concentrations in the western states are influenced by smoke from frequent large wildfires in those states and adjacent Canadian provinces (Kaulfus et al. 2017; Jaffe et al. 2020; Li et al. 2021). The annual mean $ePM_{2.5}$ is slightly higher in 2021 than that in 2020 in the central and eastern states, with an increase of about 3 $\mu g\ m^{-3}$ in many areas. The annual mean of daily $ePM_{2.5}$ have R^2 values of 0.73 and 0.70, mean biases of 0.34 and 0.71 $\mu g\ m^{-3}$, and RMSEs of 1.81 and 1.96 $\mu g\ m^{-3}$ for the year 2020 and 2021, respectively.

The EPA has set the daily $PM_{2.5}$ NAAQS as 35 $\mu g\ m^{-3}$ and set the AQI USG minimum threshold correspondingly ($\geq$35.5 $\mu g\ m^{-3}$). Figure 8 shows the number of USG+ days (days daily $PM_{2.5}$ above 35 $\mu g\ m^{-3}$) for the year 2020 and the year 2021, which are derived from daily $ePM_{2.5}$. The regions with the highest number of USG+ days are located in California and Nevada, with a maximum number of days around 50. The other regions of the United States have a small number of USG+ days, mostly less than 10. There is a gradient from high to low of the number of USG+ days from west to east, indicating the dominance of the smoke events (David et al. 2021). Comparing the two years, there are larger regions that have USG+ days in 2021 than in 2020 in the eastern CONUS. Several factors may contribute to the differences in the USG+ days pattern between the two years, such as the reduced mobile emissions due to the COVID-19 pandemic reduced $PM_{2.5}$ pollution in 2020 relative to 2021 (Straka et al. 2021), the interannual variability in biomass burning (Li et al. 2021), and the meteorological conditions (Hammer et al. 2021). The number USG+ days are much less if the daily $ePM_{2.5}$_13 data are used because it has much less data coverage than the daily $ePM_{2.5}$ data (supplement Figure S4).

Similar to the analysis we performed with $oPM_{2.5}$ (Fig. 5), we analyzed the relationship between estimated $PM_{2.5}$ data from ABI AODs (daytime $ePM_{2.5}$ versus daily $ePM_{2.5}$). Because hourly $ePM_{2.5}$ is generated for every pixel, we can do this regression analysis at the grid-level, unlike the analysis shown in Fig. 6, where due to limited ground stations, we stratified the analysis to individual states. Figure 9 shows the correlation, mean difference, and RMSD between the daytime $ePM_{2.5}$ and the daily $ePM_{2.5}$. The results are similar to those for the $oPM_{2.5}$ shown in Fig. 6. In most regions, the daytime $ePM_{2.5}$ and the daily $ePM_{2.5}$ have correlation coefficients of about 0.8 or higher. The daytime $ePM_{2.5}$ is slightly lower than the daily $ePM_{2.5}$ in most areas, about 1 $\mu g\ m^{-3}$. The notable exceptions are the Montana/Wyoming area, Texas, and the Gulf Coast of Louisiana. Both Texas (slightly positive) and Wyoming showed a similar relationship in the $oPM_{2.5}$ analysis as well. RMSDs are also higher in the western states, especially in California, Nevada, and Oregon, with magnitudes as high as 10–15 $\mu g\ m^{-3}$ in some areas. The Nevada area shows a lot of small-scale variation that needs further exploration. RMSDs are lower in the central and eastern states, about 5 $\mu g\ m^{-3}$.

The current version of the ABI AOD algorithm requires the view zenith angle to be less than 60° for high and medium quality retrievals, which causes some areas not be covered even with the combined *GOES-16* and *GOES-17* AOD. The gap in Montana and North Dakota is the region that both *GOES-16* and *GOES-17* have view zenith angle larger than 60° and therefore no AOD retrievals are available in that region. Arizona and New Mexico have the lowest correlation between the daytime and daily $ePM_{2.5}$ (correlation coefficient between 0.3 and 0.6). The surface over these two states has very little vegetation cover. The ABI AOD retrieval algorithm

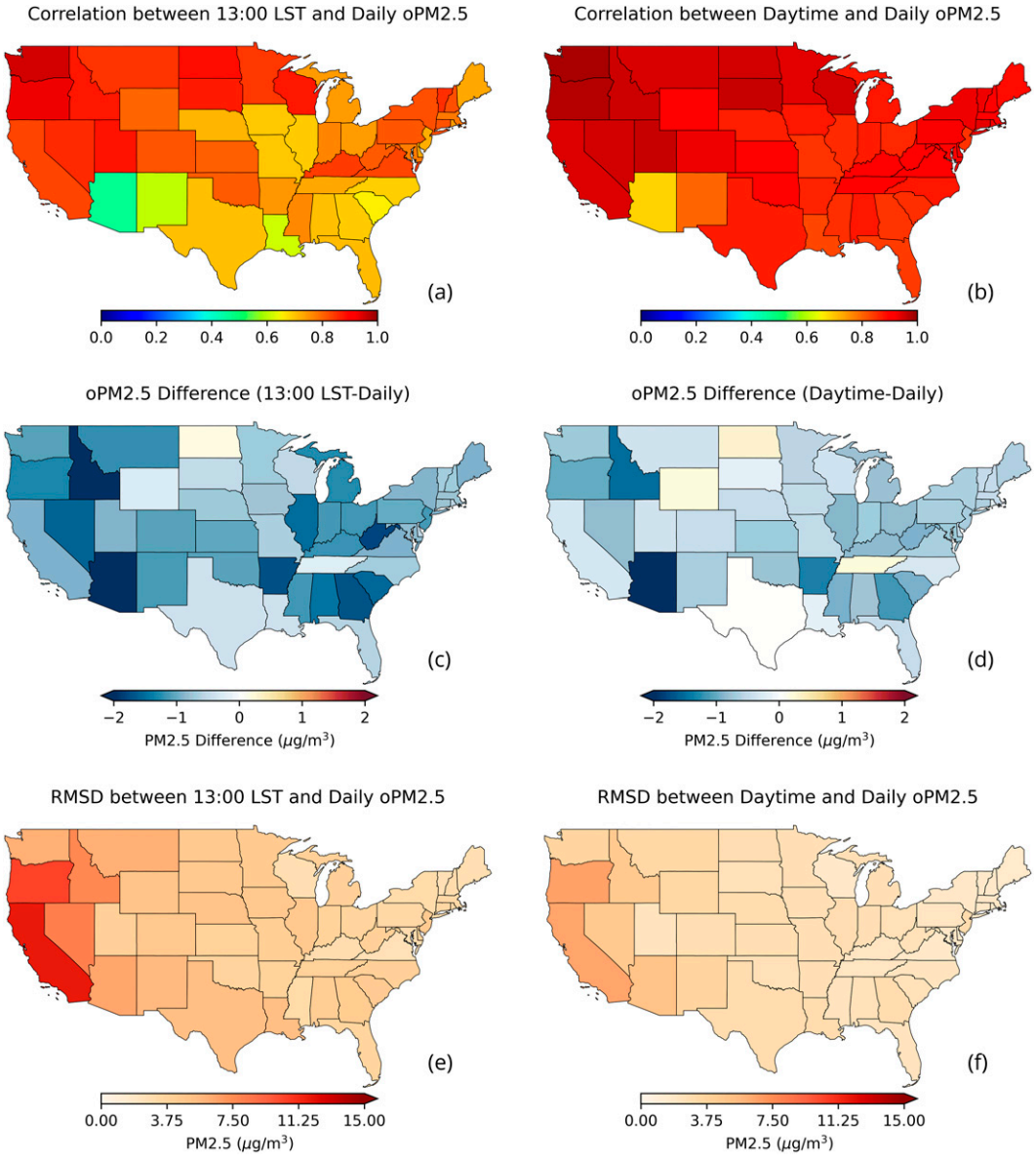

FIG. 6. (a),(b) Correlation; (c),(d) mean difference; and (e),(f) root-mean-squared difference (RMSD) between 1300 LST hourly $oPM_{2.5}$ and daily $oPM_{2.5}$, and between daytime $oPM_{2.5}$ and daily $oPM_{2.5}$.

does not work well over such surfaces and therefore AOD may have larger uncertainty (Zhang et al. 2020). Sometimes there may be no retrievals in those regions due to the surface reflectance being higher than the threshold of the AOD retrieval algorithm (see the supplement). Such uncertainties in AOD may be one of the reasons for the low correlation in these areas. On the other hand, it may be a local phenomenon, where daytime estimates are higher than daily estimates because the same relationship (lower correlation between daytime and daily $oPM_{2.5}$) is seen in the observations (Fig. 6).

The benefit of the hourly $PM_{2.5}$ estimate is that the diurnal variation of $PM_{2.5}$ can be monitored, rather than using a single daily $PM_{2.5}$ value. Figure 10 shows the map of the hour of the highest mean $ePM_{2.5}$ (the peak $ePM_{2.5}$) from the two years of hourly $ePM_{2.5}$ estimates. In the eastern United States, the peak occurs mostly in the early morning and late in the afternoon. For example, in the northeast coastal states, such as New Jersey, Massachusetts, Maryland, etc., the peak hours are around 1800 LST; many other eastern areas have peaks in the early morning at 0800 LST, such as Georgia, South Carolina, etc. indicating the dominance of transportation sector related $PM_{2.5}$ during morning and evening rush hour traffic. Along the west coast, such as California, Oregon, Washington, etc., the peak hours occur late in the morning and close to noon, around 1000–1100 LST. The pattern of the eastern U.S. peaks is in accordance with Manning et al. (2018), who reported that the

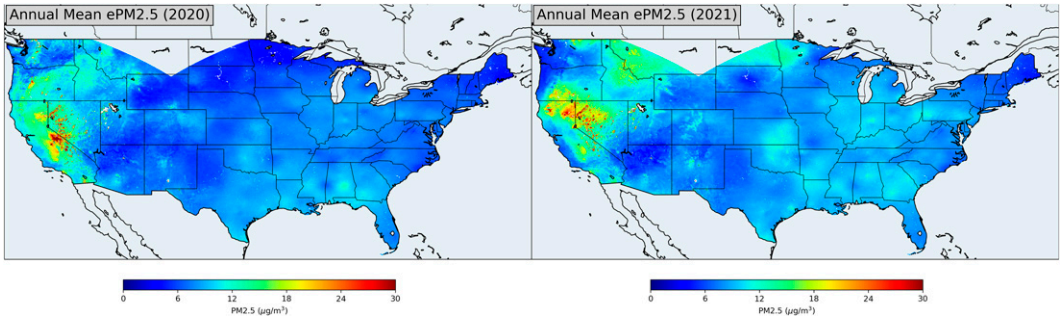

FIG. 7. Annual mean daily $ePM_{2.5}$ estimates for (left) 2020 and (right) 2021.

mean $PM_{2.5}$ tends to peak in the early morning and in the early evening in North America. The diurnal change of the mixed layer height is considered one of the main reasons for the observed diurnal pattern of $PM_{2.5}$ concentration (Manning et al. 2018). The pattern in the western United States, with high $PM_{2.5}$ around noon, does not correspond to the overall mean pattern observed by Manning et al. (2018); probably the pattern is caused by the characteristics of wildfire smoke events.

d. $PM_{2.5}$ exposure case study: Extreme fires of 2020

We calculated the number of people receiving air quality warnings at the census tracts level, based on satellite derived $PM_{2.5}$ estimates during 1 July–2 October 2020, when the fire season was extreme and persistent in California, Oregon, and Washington. We generated four different estimates, one for daily $ePM_{2.5}$, one for daytime $ePM_{2.5}$, one for daily $ePM_{2.5}$_13, and one for the 3-h $ePM_{2.5}$ rolling average. For comparison, we also calculated the number of people receiving the warnings using AirNow observations alone, without the benefit of satellite data using hourly $oPM_{2.5}$ and daily $oPM_{2.5}$. Figure 11 shows the time series of the number of people potentially warned about harmful exposure to $ePM_{2.5}$ for these six estimates, starting 1 July 2020 and ending 2 October 2020. While there is not much difference in the number of people who would have been exposed to dangerous levels of $PM_{2.5}$ concentrations based on $ePM_{2.5}$ using either the daily average (3.7 million day^{-1}) or the daytime average (4.0 million day^{-1}), the 1300 LST $ePM_{2.5}$ protects (or informs) far fewer people (2.6 million day^{-1}). The daily $ePM_{2.5}$_13 values are reflective of one observation per day and have many gaps due to clouds. In contrast, daily or daytime $ePM_{2.5}$ values have broader spatial coverage due to multiple observations. The gray line in Fig. 11 shows the number of people exposed according to the 3-h $ePM_{2.5}$ rolling mean. If forecasters were to rely on satellite data to provide warnings and alerts, having the redundancy of $ePM_{2.5}$ on hourly basis is extremely useful; potential harmful exposure to $PM_{2.5}$ reaches, on average, 1.8 million people per hour during the fire season. In contrast, only 0.17 million people per hour are informed by AirNow monitors. It should be noted that, with AirNow monitor data, we only calculated the number of people exposed to harmful levels of $PM_{2.5}$ in the census tract where the monitor is located. This was done to be consistent with how satellite data were analyzed. However, in real time applications of AirNow data, forecasters look at all the monitors located in their reporting areas and use the monitor that has the highest $PM_{2.5}$ concentration to determine if an alert has to be issued or not. If that approach is taken for all reporting areas of the CONUS, the number of people alerted for harmful levels of pollution will likely be similar to what we report for satellite data in Fig. 11.

4. Discussion and conclusions

A geographically weighted regression algorithm is used in this work to estimate hourly, daytime, and daily $PM_{2.5}$ from ABI AOD over the CONUS. The results show that daily $ePM_{2.5}$ performs better than hourly $ePM_{2.5}$, probably due to temporal averaging that removes noise in the data. The hourly

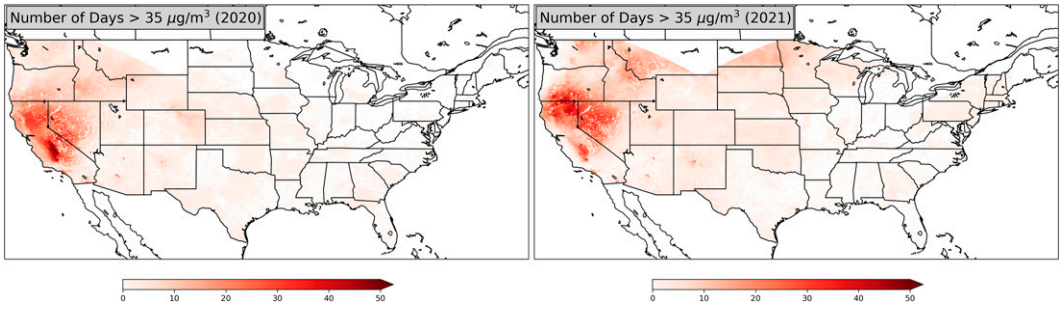

FIG. 8. Number of unhealthy for sensitive groups or higher (USG+, daily $ePM_{2.5} > 35\ \mu g\ m^{-3}$) days for (left) 2020 and (right) 2021.

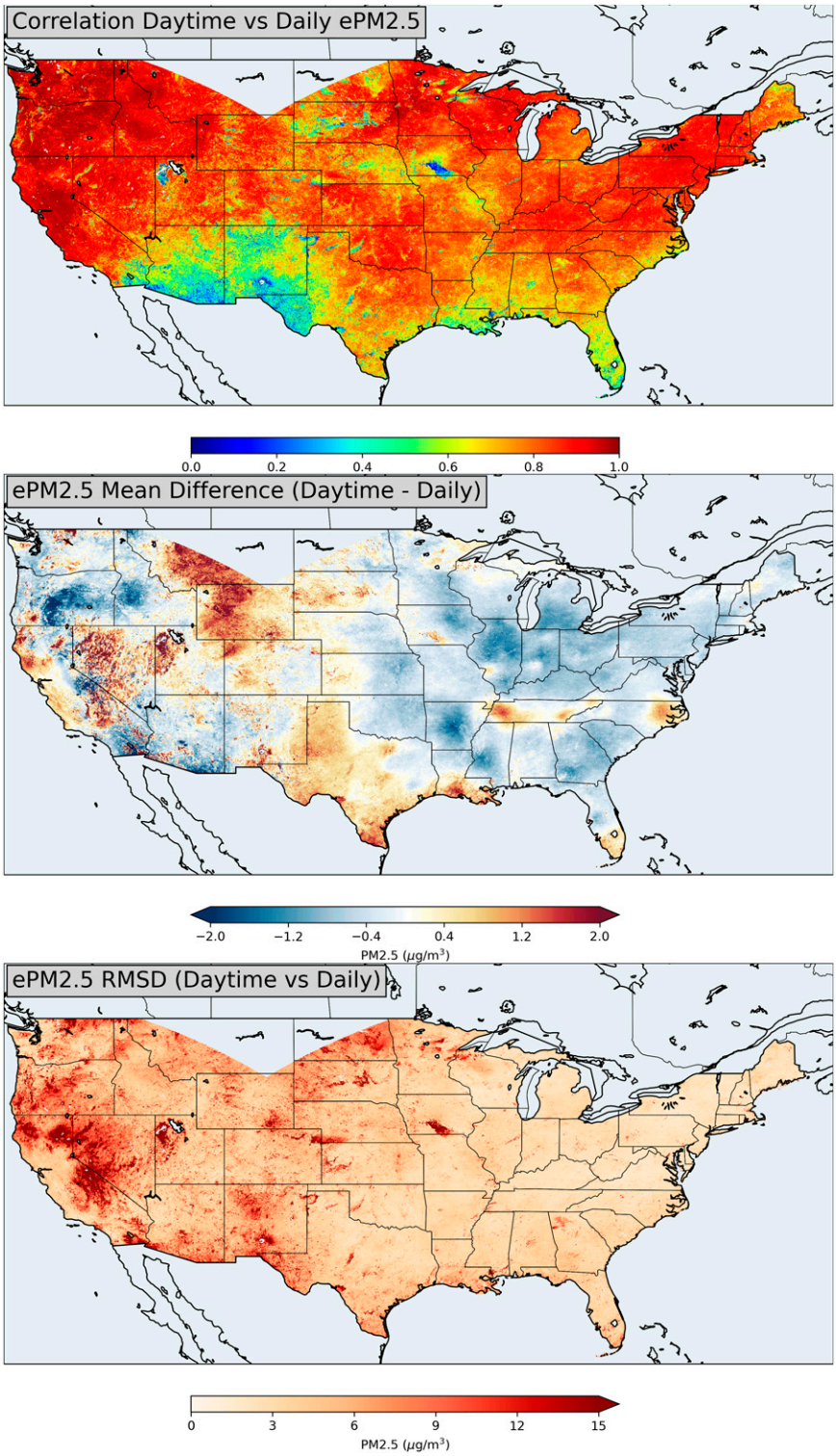

FIG. 9. (top) Correlation, (middle) mean difference, and (bottom) RMSD between daytime and daily $ePM_{2.5}$.

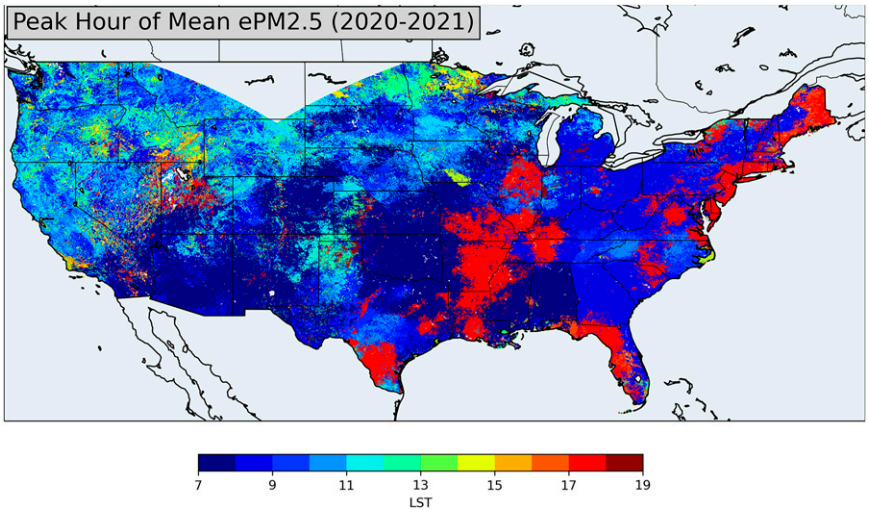

FIG. 10. Peak hour of mean $ePM_{2.5}$ derived from two years of hourly $ePM_{2.5}$.

$ePM_{2.5}$ data have an R^2 of 0.56, a mean bias of -0.04 $\mu g\ m^{-3}$, and an RMSE of 8.99 $\mu g\ m^{-3}$. The daily $ePM_{2.5}$ data have an R^2 of 0.70, a mean bias of 0.06 $\mu g\ m^{-3}$, and an RMSE of 6.31 $\mu g\ m^{-3}$. Both hourly and daily $ePM_{2.5}$ have larger negative bias in the higher $PM_{2.5}$ ranges, i.e., very unhealthy and hazardous AQI categories, while daily $ePM_{2.5}$ have lower magnitudes of mean bias than hourly $ePM_{2.5}$. $ePM_{2.5}$ do not show noticeable dependence on the distance to the nearest site for the lowest four AQI categories, but the negative biases increase with respect to increasing distances in the very unhealthy and hazardous categories. The $ePM_{2.5}$ also do not appear to have significant dependencies on land surface type.

The nowcasting ability of $ePM_{2.5}$ is evaluated by looking at the AirNow $oPM_{2.5}$ data. The relation between $oPM_{2.5}$ at 1300 LST and the daily mean, and between the daytime mean and the daily mean are analyzed, which correspond to the overpass times of polar-orbiting satellites and geostationary satellites, respectively. The results show that the daytime $oPM_{2.5}$ estimates have higher correlation coefficients (0.68–0.98 versus 0.46–0.95) and lower RMSDs (1.7–6.5 versus 2.5–11.8 $\mu g\ m^{-3}$) with the daily $oPM_{2.5}$ than the $oPM_{2.5}$ at 1300 LST have with the daily $oPM_{2.5}$. This is an indication that higher temporal resolution data from geostationary satellites can potentially better represent the daily $PM_{2.5}$.

While there is not much difference in the number of people informed about dangerous levels of $PM_{2.5}$ concentrations based on $ePM_{2.5}$ using either the daily average (3.7 million day^{-1}) or the daytime average (4.0 million day^{-1}), the 1300 LST $ePM_{2.5}$ protects (or informs) far fewer people (2.6 million day^{-1}). If forecasters were to rely on satellite data to provide warnings and alerts, having the redundancy of $ePM_{2.5}$ on hourly basis is extremely useful; information of potential harmful exposure to $PM_{2.5}$ reaches, on average, 1.8 million people per hour during

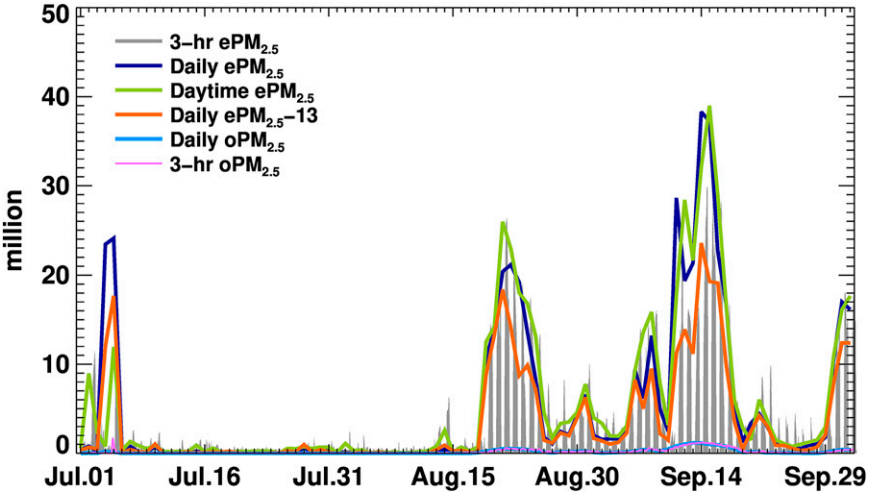

FIG. 11. Population exposed to $PM_{2.5} > 35$ $\mu g\ m^{-3}$ over CONUS (July–September 2020).

the fire season; in contrast, only 0.17 million people per hour are informed by AirNow monitors.

Operational air quality forecasters use many different sources of information including satellite products to provide local and regional warnings and watches for poor air quality. In this study, we examined the role of satellite data, specifically the difference between geostationary satellites and polar-orbiting satellites and showed that having multiple observations expands spatial coverage and improved product performance. In addition to gaps in data due to clouds, polar-orbiting satellite data are also often not timely for the forecasters who issue the forecast in the midafternoon for the next 24–48 h.

Thus far, satellite estimates of $PM_{2.5}$ data have been used in retrospective case studies of air pollution episodes and their impact on human health for long-term and short-term exposure. Geostationary satellite aerosol products have only been used, thus far, to verify hourly operational air quality forecasts to diagnose numerical model errors in physics and chemistry, especially those related to boundary layer dynamics, wind speed and direction, and anthropogenic and biomass burning emissions (Kondragunta et al. 2008, 2018). This is the first study to conduct an extensive analysis to demonstrate that satellite data when made available in Nowcasting mode can be very useful for operational forecasters when providing warnings and watches.

The study is limited by the GWR algorithm having large negative bias (56% for hourly estimates and 39% for daily estimates) for concentrations greater than 250 $\mu g\ m^{-3}$, while it performs very well for concentration ranges between 0 and 250 $\mu g\ m^{-3}$. This arises from low sampling when concentrations are high as thick smoke is misclassified as cloud. This is more serious for ABI data compared to VIIRS data because unlike VIIRS, ABI does not have deep blue channels, therefore the ABI cloud mask algorithm is less capable than that of VIIRS. Some of these pixels may be identified as low quality due to the inconsistency in different cloud mask tests, because low quality pixels are not used in the $PM_{2.5}$ estimation algorithm. One possible solution is therefore to identify such pixels and use them in the $PM_{2.5}$ estimation. Therefore, further improvements in the ABI AOD retrieval algorithms, such as cloud mask modifications and quality controls, may improve the accuracy of $PM_{2.5}$ estimates. In addition, improvements in the estimation algorithms using oversampling techniques such as SMOTE to reduce large biases in the high $PM_{2.5}$ concentration ranges will be explored.

Acknowledgments. Dr. Susan C. Anenberg and Dr. Katelyn O'Dell acknowledge the support of NOAA (Grant NA21OAR4310250). The authors thank Dr. Amy Huff (IMSG) for editorial work. The scientific results and conclusions, as well as any views or opinions expressed herein, are those of the authors and do not necessarily reflect the views of NOAA or the Department of Commerce. The views expressed in this manuscript are those of the authors alone and do not necessarily reflect the views and policies of the U.S. Environmental Protection Agency.

Data availability statement. The AIRNow $PM_{2.5}$ data are available at http://files.airnowtech.org/ (accessed 9 June 2022). The other data used for the paper are available upon request by sending email to the lead author at Hai.Zhang@noaa.gov.

REFERENCES

Brook, R. D., and Coauthors, 2010: Particulate matter air pollution and cardiovascular disease: An update to the scientific statement from the American Heart Association. *Circulation*, **121**, 2331–2378, https://doi.org/10.1161/CIR.0b013e3181dbece1.

Burnett, R. T., and Coauthors, 2014: An integrated risk function for estimating the global burden of disease attributable to ambient fine particulate matter exposure. *Environ. Health Perspect.*, **122**, 397–403, https://doi.org/10.1289/ehp.1307049.

Chu, Y., and Coauthors, 2016: A review on predicting ground $PM_{2.5}$ concentration using satellite aerosol optical depth. *Atmosphere*, **7**, 129, https://doi.org/10.3390/atmos7100129.

Chudnovsky, A. A., H. J. Lee, A. Kostinski, T. Kotlov, and P. Koutrakis, 2012: Prediction of daily fine particulate matter concentrations using aerosol optical depth retrievals from the Geostationary Operational Environmental Satellite (GOES). *J. Air Waste Manage. Assoc.*, **62**, 1022–1031, https://doi.org/10.1080/10962247.2012.695321.

Cohen, A. J., and Coauthors, 2017: Estimates and 25-year trends of the global burden of disease attributable to ambient air pollution: An analysis of data from the global burden of diseases study 2015. *Lancet*, **389**, 1907–1918, https://doi.org/10.1016/S0140-6736(17)30505-6.

David, L. M., A. R. Ravishankara, S. J. Brey, E. V. Fischer, J. Volckens, and S. Kreidenweis, 2021: Could the exception become the rule? 'Uncontrollable' air pollution events in the US due to wildland fires. *Environ. Res. Lett.*, **16**, 34029, https://doi.org/10.1088/1748-9326/abe1f3.

Di, Q., and Coauthors, 2019: An ensemble-based model of $PM_{2.5}$ concentration across the contiguous United States with high spatiotemporal resolution. *Environ. Int.*, **130**, 104909, https://doi.org/10.1016/j.envint.2019.104909.

Engel-Cox, J. A., C. H. Holloman, B. W. Coutant, and R. M. Hoff, 2004: Qualitative and quantitative evaluation of MODIS satellite sensor data for regional and urban scale air quality. *Atmos. Environ.*, **38**, 2495–2509, https://doi.org/10.1016/j.atmosenv.2004.01.039.

Fotheringham, A., C. Brunsdon, and M. Charlton, 2002: *Geographically Weighted Regression: The Analysis of Spatially Varying Relationships*. John Wiley & Sons Inc., 288 pp.

Geng, G., and Coauthors, 2018: Satellite-based daily $PM_{2.5}$ estimates during fire seasons in Colorado. *J. Geophys. Res. Atmos.*, **123**, 8159–8171, https://doi.org/10.1029/2018JD028573.

Gupta, P., and S. A. Christopher, 2009: Particulate matter air quality assessment using integrated surface, satellite, and meteorological products: Multiple regression approach. *J. Geophys. Res.*, **114**, D14205, https://doi.org/10.1029/2008JD011496.

Hammer, M. S., and Coauthors, 2021: Effects of COVID-19 lockdowns on fine particulate matter concentrations. *Sci. Adv.*, **7**, eabg7670, https://doi.org/10.1126/sciadv.abg7670.

Hasti, T., R. Tibshirani, and J. Friedman, 2017: *The Elements of Statistical Learning: Data Mining, Inference, and Prediction*. 2nd ed. Springer, 745 pp.

Hoff, R. M., and S. A. Christopher, 2009: Remote sensing of particulate pollution from space: Have we reached the promised

land? *J. Air Waste Manage. Assoc.*, **59**, 645–675, https://doi.org/10.3155/1047-3289.59.6.645.

Hu, X., and Coauthors, 2013: Estimating ground-level $PM_{2.5}$ concentrations in the southeastern U.S. using geographically weighted regression. *Environ. Res.*, **121**, 1–10, https://doi.org/10.1016/j.envres.2012.11.003.

——, and Coauthors, 2014: Estimating ground-level $PM_{2.5}$ concentrations in the Southeastern United States using MAIAC AOD retrievals and a two-stage model. *Remote Sens. Environ.*, **140**, 220–232, https://doi.org/10.1016/j.rse.2013.08.032.

——, J. H. Belle, X. Meng, A. Wildani, L. A. Waller, M. J. Strickland, and Y. Liu, 2017: Estimating $PM_{2.5}$ concentrations in the conterminous United States using the random forest approach. *Environ. Sci. Technol.*, **51**, 6936–6944, https://doi.org/10.1021/acs.est.7b01210.

Hu, Z., 2009: Spatial analysis of MODIS aerosol optical depth, $PM_{2.5}$, and chronic coronary heart disease. *Int. J. Health Geogr.*, **8**, 27, https://doi.org/10.1186/1476-072X-8-27.

Huff, A. K., S. Kondragunta, H. Zhang, I. Laszlo, M. Zhou, V. Caicedo, R. Delgado, and R. Levy, 2021: Tracking smoke from a prescribed fire and its impacts on local air quality using temporally resolved *GOES-16* ABI aerosol optical depth (AOD). *J. Atmos. Oceanic Technol.*, **38**, 963–976, https://doi.org/10.1175/JTECH-D-20-0162.1.

Ichoku, C., D. A. Chu, S. Mattoo, Y. J. Kaufman, L. A. Remer, D. Tanré, I. Slutsker, and B. N. Holben, 2002: A spatiotemporal approach for global validation and analysis of MODIS aerosol products. *Geophys. Res. Lett.*, **29**, 8006, https://doi.org/10.1029/2001GL013206.

Jaffe, D. A., S. M. O'Neill, N. K. Larkin, A. L. Holder, D. L. Peterson, J. E. Halofsky, and A. G. Rappold, 2020: Wildfire and prescribed burning impacts on air quality in the United States. *J. Air Waste Manage. Assoc.*, **70**, 583–615, https://doi.org/10.1080/10962247.2020.1749731.

Just, A. C., K. B. Arfer, J. Rush, M. Dorman, A. Shtein, A. Lyapustin, and I. Kloog, 2020: Advancing methodologies for applying machine learning and evaluating spatiotemporal models of fine particulate matter ($PM_{2.5}$) using satellite data over large regions. *Atmos. Environ.*, **239**, 117649, https://doi.org/10.1016/j.atmosenv.2020.117649.

Kaulfus, A. S., U. Nair, D. Jaffe, S. A. Christopher, and S. Goodrick, 2017: Biomass burning smoke climatology of the United States: Implications for particulate matter air quality. *Environ. Sci. Technol.*, **51**, 112731–112741, https://doi.org/10.1021/acs.est.7b03292.

Kelly, J. T., and Coauthors, 2021: Examining PM2.5 concentrations and exposure using multiple models. *Environ. Res.*, **196**, 110432, https://doi.org/10.1016/j.envres.2020.110432.

Kloog, I., P. Koutrakis, B. A. Coull, H. J. Lee, and J. Schwartz, 2011: Assessing temporally and spatially resolved $PM_{2.5}$ exposures for epidemiological studies using satellite aerosol optical depth measurements. *Atmos. Environ.*, **45**, 6267–6275, https://doi.org/10.1016/j.atmosenv.2011.08.066.

Kondragunta, S., and Coauthors, 2008: Air quality forecast verification using satellite data. *J. Appl. Meteor. Climatol.*, **47**, 425–442, https://doi.org/10.1175/2007JAMC1392.1.

——, H. Zhang, P. Ciren, I. Laszlo, and D. Tong, 2018: Tracking dust storms using the latest satellite technology: The Rapid Refresh GOES-16 Advanced Baseline Imager. *EM: The Magazine for Environmental Managers*, A&WMA, May 2018, https://pubs.awma.org/flip/EM-May-2018/kondragunta.pdf.

——, I. Laszlo, H. Zhang, P. Ciren, and A. Huff, 2020: Air quality applications of ABI aerosol products from the GOES-R series. *The GOES-R Series: A New Generation of Geostationary Environmental Satellites*, S. J. Goodman et al., Eds., Elsevier, 203–217.

Lee, H. J., Y. Liu, B. A. Coull, J. Schwartz, and P. Koutrakis, 2011: A novel calibration approach of MODIS AOD data to predict $PM_{2.5}$ concentrations. *Atmos. Chem. Phys.*, **11**, 7991–8002, https://doi.org/10.5194/acp-11-7991-2011.

Levy, R. C., S. Mattoo, L. A. Munchak, L. A. Remer, A. M. Sayer, F. Patadia, and N. C. Hsu, 2013: The collection 6 MODIS aerosol products over land and ocean. *Atmos. Meas. Tech.*, **6**, 2989–3034, https://doi.org/10.5194/amt-6-2989-2013.

Li, Y., D. Tong, S. Ma, X. Zhang, S. Kondragunta, F. Li, and R. Saylor, 2021: Dominance of wildfires impact on air quality exceedances during the 2020 record-breaking wildfire season in the United States. *Geophys. Res. Lett.*, **48**, e2021GL094908, https://doi.org/10.1029/2021GL094908.

Liu, H., L. A. Remer, J. Huang, H.-C. Huang, S. Kondragunta, I. Laszlo, M. Oo, and J. M. Jackson, 2014: Preliminary evaluation of S-NPP VIIRS aerosol optical thickness. *J. Geophys. Res. Atmos.*, **119**, 3942–3962, https://doi.org/10.1002/2013JD020360.

Liu, Y., J. Sarnat, V. Kilaru, D. K. Jacob, and P. Outrakis, 2005: Estimating ground-level $PM_{2.5}$ in the eastern United States using satellite remote sensing. *Environ. Sci. Technol.*, **39**, 3269–3278, https://doi.org/10.1021/es049352m.

Ma, Z., X. Hu, L. Huang, J. Bi, and Y. Liu, 2014: Estimating ground-level $PM_{2.5}$ in China using satellite remote sensing. *Environ. Sci. Technol.*, **48**, 7436–7444, https://doi.org/10.1021/es5009399.

Manning, M. I., R. V. Martin, C. Hasenkopf, J. Flasher, and C. Li, 2018: Diurnal patterns in global fine particulate matter concentration. *Environ. Sci. Technol. Lett.*, **5**, 687–691, https://doi.org/10.1021/acs.estlett.8b00573.

Martin, R. V., 2008: Satellite remote sensing of surface air quality. *Atmos. Environ.*, **42**, 7823–7843, https://doi.org/10.1016/j.atmosenv.2008.07.018.

Mhawish, A., T. Banerjee, M. Sorek-Hamer, M. Bilal, A. I. Lyapustin, R. Chatfield, and D. M. Broday, 2020: Estimation of high-resolution $PM_{2.5}$ over the Indo-Gangetic Plain by fusion of satellite data, meteorology, and land use variables. *Environ. Sci. Technol.*, **54**, 7891–7900, https://doi.org/10.1021/acs.est.0c01769.

Miller, L., and X. Xu, 2018: Ambient $PM_{2.5}$ human health effects—Findings in China and research directions. *Atmosphere*, **9**, 424, https://doi.org/10.3390/atmos9110424.

NOAA/NESDIS, 2018: GOES-R Advanced Baseline Imager (ABI) Algorithm Theoretical Basis Document for Suspended Matter/Aerosol Optical Depth and Aerosol Size Parameter. NOAA/NESDIS, Center for Satellite Applications and Research, 112 pp., https://www.star.nesdis.noaa.gov/smcd/spb/aq/AerosolWatch/docs/GOES-R_ABI_AOD_ATBD_V4.2_20180214.pdf.

O'Dell, K., K. Bilsback, B. Ford, S. E. Martenies, S. Magzamen, E. V. Fischer, and J. R. Pierce, 2021: Estimated mortality and morbidity attributable to smoke plumes in the United States: Not just a western U.S. problem. *GeoHealth*, **5**, e2021GH000457, https://doi.org/10.1029/2021GH000457.

Park, S. J., and Coauthors, 2020: Estimation of spatially continuous daytime particulate matter concentrations under all sky conditions through the synergistic use of satellite-based AOD

and numerical models. *Sci. Total Environ.*, **713**, 136516, https://doi.org/10.1016/j.scitotenv.2020.136516.

Park, Y., B. Kwon, J. Heo, X. Hu, Y. Liu, and T. Moon, 2020: Estimating $PM_{2.5}$ concentration of the conterminous United States via interpretable convolutional neural networks. *Environ. Pollut.*, **256**, 113395, https://doi.org/10.1016/j.envpol.2019.113395.

Pope, C. A., III, and D. W. Dockery, 2006: Health effects of fine particulate air pollution: Lines that connect. *J. Air Waste Manage. Assoc.*, **56**, 709–742, https://doi.org/10.1080/10473289.2006.10464485.

Schmit, T. J., M. M. Gunshor, W. P. Menzel, J. J. Gurka, J. Li, and A. S. Bachmeier, 2005: Introducing the next-generation advanced baseline imager on GOES-R. *Bull. Amer. Meteor. Soc.*, **86**, 1079–1096, https://doi.org/10.1175/BAMS-86-8-1079.

——, S. S. Lindstrom, J. J. Gerth, and M. M. Gunshor, 2017: Applications of the 16 spectral bands on the Advanced Baseline Imager (ABI). *J. Oper. Meteor.*, **6**, 33–46, https://doi.org/10.15191/nwajom.2018.0604.

She, Q., and Coauthors, 2020: Satellite-based estimation of hourly $PM_{2.5}$ levels during heavy winter pollution episodes in the Yangtze River Delta, China. *Chemosphere*, **239**, 124678, https://doi.org/10.1016/j.chemosphere.2019.124678.

Song, W., H. Jia, J. Huang, and Y. Zhang, 2014: A satellite-based geographically weighted regression model for regional $PM_{2.5}$ estimation over the Pearl River Delta region in China. *Remote Sens. Environ.*, **154**, 1–7, https://doi.org/10.1016/j.rse.2014.08.008.

Southerland, V. A., M. Brauer, A. Mohegh, M. S. Hammer, A. van Donkelaar, R. V. Martin, J. S. Apte, and S. C. Anenberg, 2022: Global urban temporal trends in fine particulate matter ($PM_{2\cdot5}$) and attributable health burdens: Estimates from global datasets. *Lancet Planet. Health*, **6**, E139–E146, https://doi.org/10.1016/S2542-5196(21)00350-8.

Straka, W., III, S. Kondragunta, Z. Wei, H. Zhang, S. D. Miller, and A. Watts, 2021: Examining the economic and environmental impacts of COVID-19 using Earth observation data. *Remote Sens.*, **13**, 5, https://doi.org/10.3390/rs13010005.

Van Donkelaar, A., R. V. Martin, and R. J. Park, 2006: Estimating ground-level $PM_{2.5}$ using aerosol optical depth determined from satellite remote sensing. *J. Geophys. Res.*, **111**, D21201, https://doi.org/10.1029/2005JD006996.

——, ——, A. N. Pasch, J. J. Szykman, L. Zhang, Y. X. Wang, and D. Chen, 2012: Improving the accuracy of daily satellite-derived ground-level fine aerosol concentration estimates for North America. *Environ. Sci. Technol.*, **46**, 112971–112978, https://doi.org/10.1021/es3025319.

Vu, B. N., J. Bi, W. Wang, A. Huff, S. Kondragunta, and Y. Liu, 2022: Application of geostationary satellite and high-resolution meteorology data in estimating hourly PM2.5 levels during the Camp Fire episode in California. *Remote Sens. Environ.*, **271**, 112890, https://doi.org/10.1016/j.rse.2022.112890.

Xiao, Q., H. H. Chang, G. Geng, and Y. Liu, 2018: An ensemble machine-learning model to predict historical $PM_{2.5}$ concentrations in China from satellite data. *Environ. Sci. Technol.*, **52**, 132260–132269, https://doi.org/10.1021/acs.est.8b02917.

Xu, J., and Coauthors, 2015: Estimating ground-level $PM_{2.5}$ in eastern China using aerosol optical depth determined from the GOCI satellite instrument. *Atmos. Chem. Phys.*, **15**, 132133–132144, https://doi.org/10.5194/acp-15-13133-2015.

Zhang, H., and S. Kondragunta, 2021: Daily and hourly surface PM2.5 estimation from satellite AOD. *Earth Space Sci.*, **8**, e2020EA001599, https://doi.org/10.1029/2020EA001599.

——, R. M. Hoff, and J. A. Engel-Cox, 2009: The relation between Moderate Resolution Imaging Spectroradiometer (MODIS) aerosol optical depth and $PM_{2.5}$ over the United States: A geographical comparison by EPA regions. *J. Air Waste Manage. Assoc.*, **59**, 1358–1369, https://doi.org/10.3155/1047-3289.59.11.1358.

——, and Coauthors, 2016: An enhanced VIIRS aerosol optical thickness (AOT) retrieval algorithm over land using a global surface reflectance ratio database. *J. Geophys. Res. Atmos.*, **121**, 102717–102738, https://doi.org/10.1002/2016JD024859.

——, S. Kondragunta, I. Laszlo, and M. Zhou, 2020: Improving GOES advanced baseline imager (ABI) aerosol optical depth (AOD) retrievals using an empirical bias correction algorithm. *Atmos. Meas. Tech.*, **13**, 5955–5975, https://doi.org/10.5194/amt-13-5955-2020.

Zheng, Y., Q. Zhang, Y. Liu, G. Geng, and K. He, 2016: Estimating ground-level $PM_{2.5}$ concentrations over three megalopolises in China using satellite-derived aerosol optical depth measurements. *Atmos. Environ.*, **124**, 232–242, https://doi.org/10.1016/j.atmosenv.2015.06.046.

Zhou, M., and Coauthors, 2021: Nighttime smoke aerosol optical depth over U.S. rural areas: First retrieval from VIIRS moonlight observations. *Remote Sens. Environ.*, **267**, 112717, https://doi.org/10.1016/j.rse.2021.112717.